Optics & Laser Technology 146 (2022) 107571

Contents lists available at ScienceDirect

Optics and Laser Technology

journal homepage: www.elsevier.com/locate/optlastec

Simultaneously surface- and edge-emitting plasmonic laser operating in the near-infrared region

Zihad Azad, Muhammad Anisuzzaman Talukder *

Department of Electrical and Electronic Engineering, Bangladesh University of Engineering and Technology, Dhaka 1205, Bangladesh

ARTICLE INFO

Keywords:
Plasmonic laser
Surface plasmon polariton
Localized surface plasmon
Plasmonic collimator
Edge emission
Surface emission

ABSTRACT

Near-infrared (IR) plasmonic lasers are a crucial stepping stone toward building sustainable nanoscale optoelectronic circuitry. Nevertheless, plasmonic lasers are at their infancy, and optimized designs for improved characteristics and novel applications are essential. We design an efficient plasmonic laser that simultaneously works in the near-IR region as a surface- and edge-emitting laser with collimated far-field beam pattern. While the surface emission is enhanced with a planar two-dimensional (2D) metal nanohole array (NHA) interfaced with the gain medium, the edge emission is enhanced with a 2D array of grooves. Additionally, 2D NHA or grooves on the metal layer collimate the far-field beam pattern of surface emission in the forward and backward direction, respectively. By contrast, the edge emission diverges at the far-field with an angle-resolved beam pattern from -90° to 90°. We propose and design a plasmonic collimator that uses groove-aperture nanostructures carved on gold slabs mounted on the laser facet to collimate the far-field beam patterns for edge emission. We determine the optimal dimensional parameters of the collimator. The optimized collimator produces a far-field beam that is focused to a narrow spot of $3^\circ \times 4^\circ$ only.

1. Introduction

Plasmonic lasers are essential for their ability of miniaturization and confining light within subwavelength dimensions [1,2]. Plasmonic lasers benefit from the excitation of plasmonic modes such as surface plasmon polaritons (SPPs) and localized surface plasmons (LSPs) [3]. While the excitation of plasmonic modes lies within the core of such lasers' principle of operation, these modes often lead to a substantial loss of energy within metal structures required to excite them [4]. Hence, the efficiency of plasmonic lasers is a severe concern. The divergent far-field pattern due to a wavevector mismatch between the plasmonic and radiative modes is also a challenge to address for plasmonic lasers [5]. However, the far-field pattern of surface-emitting plasmonic lasers can be improved using two-dimensional (2D) plasmonic structure arrays that induce constructive interference between the propagating wavefronts at the far-field [6].

Planar-interfaced plasmonic lasers are usually optically pumped in the direction normal to the gain medium [7]. They emit from surfaces either in the forward or backward direction to the incident pump beam while the excited SPPs propagate in the transverse plane along the metal–gain medium interface. In a symmetric nanostructured metal-gain layer interface, SPPs propagate equally in both transverse directions. While the excitation of plasmonic modes is crucially essential to confine lasing light within the cavity, they incur massive loss since a significant amount of energy is not transformed into radiative modes [8,9]. To make a plasmonic laser efficient, we must minimize the loss due to decaying SPPs. Therefore, either the coupling of light into SPPs must be minimized, or the light coupled to SPPs must emit as a radiative mode to increase the efficiency of plasmonic lasers. However, the first approach is contrary to such lasers' fundamental principle, and hence, cannot be taken as a recourse.

Plasmonic modes can be decoupled into radiative modes from the edges of an appropriately designed plasmonic structure [10]. Conversely, lasing light propagates in the axial or longitudinal direction in the gain medium and couples out from the edges in an edge-emitting laser. Flynn et al. reported edge emission from an axially-pumped planar plasmonic laser where a gold layer sandwiched between two arrays of quantum well stacks generates long-range SPPs [11]. The SPPs transform into radiative modes and emit coherent lasing from the edge. Jin et al. also proposed a high power edge-emitting plasmonic laser recently [12]. A quantum cascade laser (QCL) ridge microcavity is split up into several smaller cavities in their work. The SPPs propagating in each

* Corresponding author.
E-mail address: anis@eee.buet.ac.bd (M.A. Talukder).

https://doi.org/10.1016/j.optlastec.2021.107571
Received 25 March 2021; Received in revised form 1 September 2021; Accepted 25 September 2021
Available online 8 October 2021

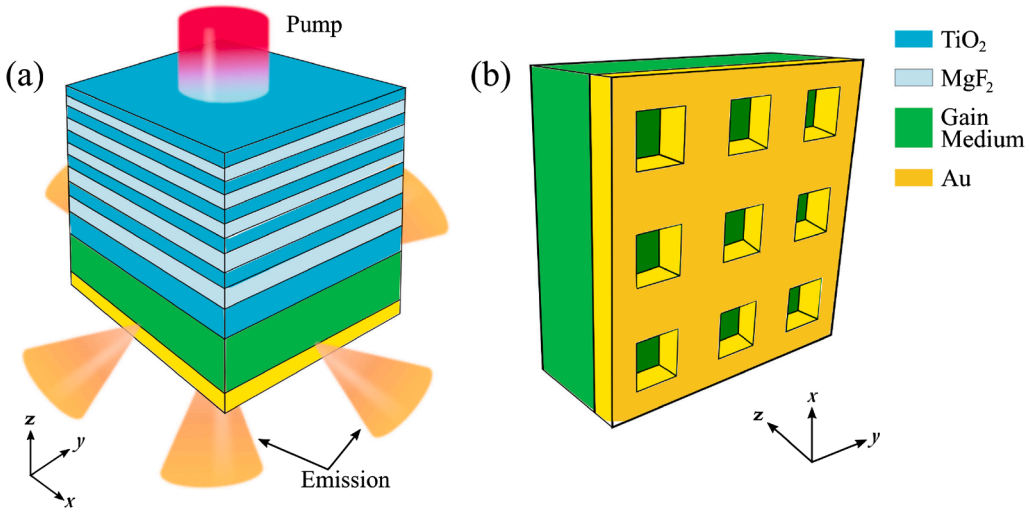

Fig. 1. (a) Perspective view of a parallel plane plasmonic laser with 2D NHA. Five alternating layers of TiO_2 and MgF_2 superposed on an extra spacer layer of TiO_2 form the 1-D PhC. The device is pumped from the PhC-end and emits from the NHA as well as all four sides of the device. (b) Schematic illustration of an IR-140 embedded gain medium interfaced with a gold layer perforated with 2D NHA. The 170 nm × 170 nm nanoholes are separated from one another by 350 nm on both directions.

cavity are synchronized with one another via phase-locking with an overarching hybrid plasmonic wave sustained in the medium surrounding the cavities. This configuration results in a constructive interference effect along the direction of edge emission. Although much research has been conducted on edge-emitting semiconductor lasers [13–15], similar endeavors in the field of plasmon-mediated lasers have been scarce, notably nothing of those emitting simultaneously from the surface and the edge.

This work shows that the excited in-plane SPPs of a parallel plane plasmonic laser with 2D nanohole array (NHA) can induce lasing from the edges in the transverse directions. Such an approach of exploiting SPPs for edge emission, in addition to the usual surface emission, will decrease loss, and hence, increase the lasing efficiency. We design a parallel plane plasmonic laser that emits from the surface and edge simultaneously. We also develop design principles to optimize the surface and edge emissions. Although the edge-emission intensity is smaller than the surface-emission intensity, we can improve the former following a systematic design principle, as presented in this work. The surface-emission intensifies when metal nanoholes are equally spaced in both transverse directions, inducing SPPs in both transverse directions equally and resulting in a constructive interference of the radiative modes at the far-field. By contrast, the edge emission enhances when metal nanoholes have unequal periodicity in the transverse directions, suppressing SPPs in one and exciting in the other transverse direction. We show that the number of nanoholes in the metal layer determines the surface emission and an increase in the number of nanoholes converges the far-field pattern. On the other hand, the edge emission does not depend significantly on the nanoholes' number in the metal layer. Additionally, the edge emission enhances when an array of grooves replaces the 2D NHA.

We show that the diverged far-field pattern of edge emission can be engineered and improved by employing a groove-aperture plasmonic collimation scheme. We use the particle swarm optimization (PSO) technique to determine the optimized collimator parameters. The optimized structure collimates the edge emission far-field to a spot of $3^\circ \times 4^\circ$ only. This work also shows how a plasmonic laser can be optimized for either surface emission, edge emission, or both. The presented analysis will be crucial for developing plasmonic lasers, especially in an optoelectronic circuit where the added benefit of emission from multiple facets can be helpful.

The rest of the paper is organized as follows: Section 2 presents the planar plasmonic laser and the simulation approaches. Section 2 also shows and discusses the surface- and edge-emission spectra with a discussion about the relation between the edge emission and the incident pump intensity and population dynamics. Section 3 presents the reconfiguration of the laser structure and replacement of the 2D NHA by grooves for enhanced edge emission. Section 4 discusses the edge-emission far-field pattern and our approach to engineer it for convergence. Finally, Section 5 draws conclusions on the findings.

2. Surface- and edge-emitting plasmonic laser

2.1. Structure and simulation approach

The plasmonic laser shown in the schematic illustration of Fig. 1 is promising for its ability to produce efficient lasing and collimated far-field pattern [6]. The laser structure uses a 2D NHA interfaced with the gain medium to induce plasmonic modes and an enhanced pump-gain medium interaction. A metallic NHA underneath and a one-dimensional (1D) photonic crystal (PhC) atop the gain medium help the lasing emission couple to the forward direction with respect to the incident pump beam, i.e., in the negative z-direction, as shown in Fig. 1. The 2D symmetric NHA also helps to achieve a converged far-field pattern. The structure is illuminated from above with a normally incident, ultra-short 40-fs plane wave pulse, centered at 800 nm.

The finite difference time domain numerical technique has been used to solve Maxwell's equations to determine the dynamics due to the incident pump beam on the gain medium and the lasing emission. A mesh size of 10 nm has been used in the simulations of this work throughout the simulation domain except a small region around the metal-gain medium interface, where a finer mesh of 3.5 nm has been used to capture the effect of plasmonics better. The simulation domain is 6 μm in the z-direction, including the pump and the entire laser structure. A section of the structure containing seven nanoholes in the x-direction and one nanohole in the y-direction has been simulated. The Bloch boundary condition has been applied in the y-direction and perfectly matched layer boundary condition in the x- and z-directions.

The gain medium is composed of polyurethane (PU) material embedded with IR-140 dye molecules. We model the IR-140 fluorescent molecules employing a four-level two-electron model [16]. We model the frequency-dependent optical properties of different layer materials using a multi-coefficient model, which yields a better fit than the conventional Lorentz-Drude model [17]. The optical constants of the layer materials and the lifetimes of the gain medium electronic states are

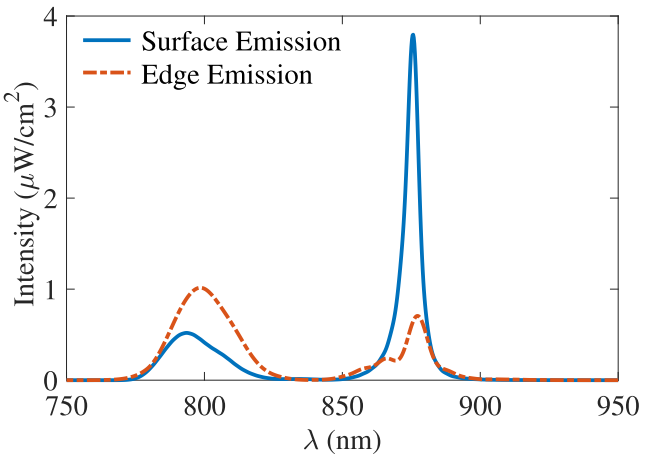

Fig. 2. Surface-emission spectrum in the forward direction and edge-emission spectrum from one of the edges.

taken from Ref. [6]. The layer thicknesses and other dimensional parameters of the structure are the same as described in Refs. [6,7].

2.2. Surface emission

The parallel plane interfaced plasmonic laser of Fig. 1 produces efficient surface emission in the forward direction. The surface-emission characteristics of such a plasmonic laser have been investigated in Refs. [6,7]. Here, Fig. 2 shows a near-field surface-emission spectrum in the forward direction. We find that the laser has a surface-emission peak at 875 nm in the forward direction with a suppressed pump beam centered at 790 nm.

2.3. Edge emission

Now, since such a plasmonic laser couples lasing light to SPP modes, there will be significant energy propagating along the metal-gain medium interface. The SPPs that reach the edges of the structure may decouple to radiative modes [12]. Therefore, it is worthy of investigating whether the parallel plane plasmonic laser with a 2D NHA emits light from the edges, although primarily designed for lasing from the surface in the forward direction. We calculate the near-field light intensity that crosses through an *x*-*z* or *y*-*z* plane at a distance of 0.5 μm from the plasmonic laser's edges in the transverse direction. Fig. 2 shows the near-field emission spectrum from one of the edges. We note that the laser emits significantly from one of the edges, although not as strongly as from the surface in the forward direction.

The emission spectrum from the edge is red-shifted from that of the surface. While the peak of surface emission occurs at $\lambda_0 = 875$ nm, the edge-emission mode is centered at $\lambda_0 = 876$ nm. The surface- and edge-emission spectra are different since the two radiative modes originate in response to slightly different surface-bound modes. The edge emission evolves from the direct conversion of SPPs from the metal-gain medium interface, while the gap plasmon modes excited inside nanoholes contribute to the surface-emission mode [18]. We note that the pump energy emits more from the edge than from the surface. The pump pulse is suppressed in the forward direction due to the 1D PhC Bragg reflector. Also, the edge-emitting peak is approximately 90% smaller than the surface-emitting peak, and its linewidth is relatively far more diffuse, showing a lack of spectral coherence.

2.3.1. Population inversion and lasing threshold

Although there is noticeable emission from the edge, it requires further investigation to determine whether the emission is due to the lasing action. Therefore, the relation between the edge emission and the population inversion of the gain medium has been investigated here. The dependence of the edge emission on the threshold pump intensity has also been examined. Fig. 3(a) presents the pump pulse and the generation of lasing from one of the edges. The lasing emission lags behind the pump pulse as the build-up of population inversion requires time. Fig. 3(a) also shows the normalized population dynamics of the lower and upper lasing levels, N_1 and N_2, respectively. The population inversion occurs at $t \approx 85$ fs and becomes steady at $t \approx 400$ fs after the initial transient dynamics decay. The dependence of the edge emission on the pump pulse and population inversion indicates that it is indeed lasing emission.

This work also investigates the change in edge-emission intensity (I_{edge}) with input pump intensity (I_{pump}) to determine the threshold behavior, which is another phenomenon exhibited by a lasing emission. Fig. 3(b) shows that $I_{\text{edge}} \approx 0$ when $I_{\text{pump}} \lessapprox 2$ μW/cm^2. However, for $I_{\text{pump}} > 2$ μW/cm^2, I_{edge} rises sharply with I_{pump} up until a critical value of 20 μW/cm^2. For $I_{\text{pump}} > 23$ μW/cm^2, I_{edge} begins to saturate, which is a characteristic of lasing action. When compared to surface emission, the edge emission requires much greater pump energy to obtain equal intensity.

2.3.2. Far-field profile

The far-field pattern of surface emission from a parallel plane plasmonic laser with 2D NHA converges to a narrow spot of 1°×1° only [6]. The surface emission also converges to a single dominant lobe at the far-field, collimating the energy significantly. By contrast, the far-field pattern of the edge emission is quite diverge, as shown in Fig. 4. We find that, in the vertical *z*-direction, the divergence angle (θ) spans the entire range from $-90°$ to $+90°$. The 2D field profile shows energy being dispersed among several lobes along the vertical line, which is also evident from the angle-resolved far-field profile. However, in the lateral

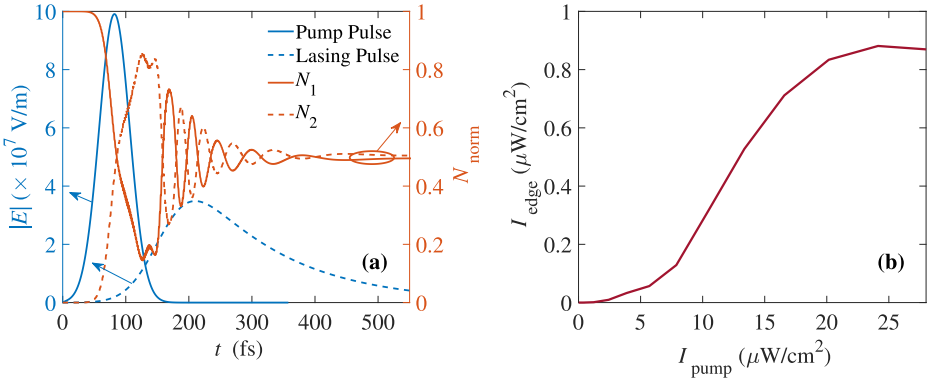

Fig. 3. (a) Time-resolved evolution of the pump pulse, edge emission, and normalized population densities of lower (N_1) and upper lasing levels (N_2). (b) Edge-emission intensity (I_{edge}) vs. incident pump intensity (I_{pump}).

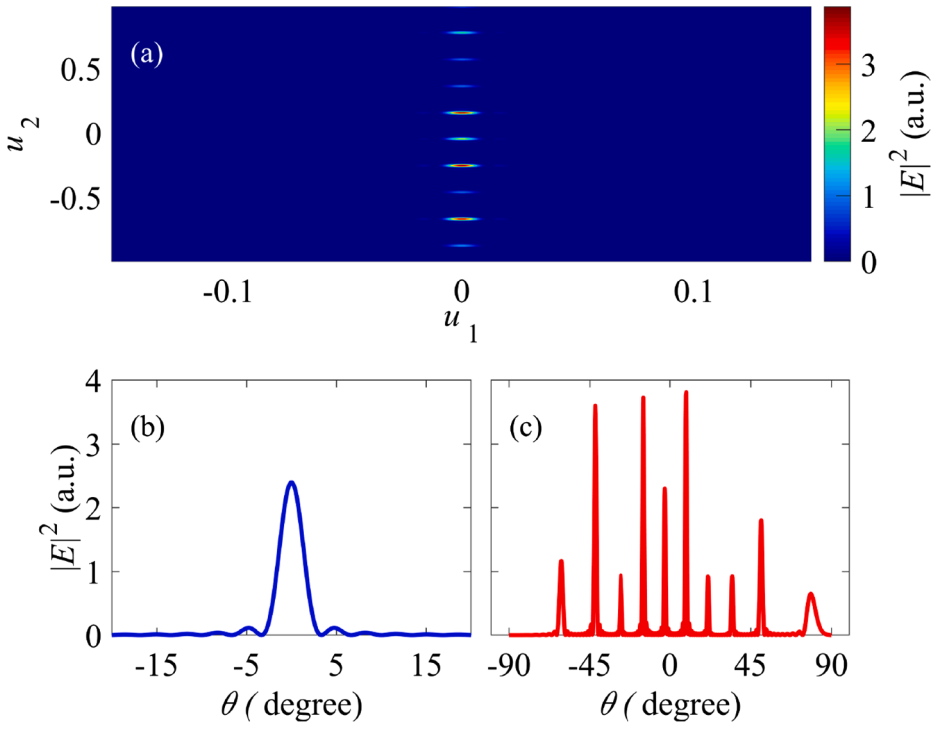

Fig. 4. (a) Far-field intensity ($|E|^2$) distribution of the uncollimated beam at lasing wavelength $\lambda_0 = 876$ nm. Here, u_1 and u_2 correspond to the y- and z-axis, respectively, at the far-field, (b) far-field $|E|^2$ against divergence angle (θ) in the x- or y-direction, and (c) far-field $|E|^2$ against θ in the z–direction.

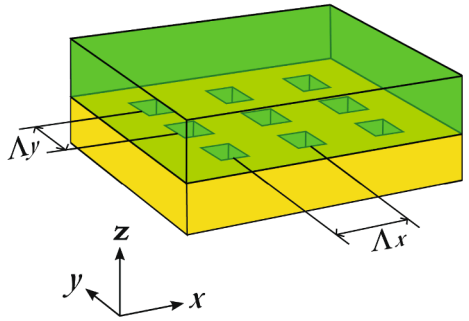

Fig. 5. Schematic illustration of restructured NHA. The nanohole periodicity in the x- and y-directions, i.e., Λ_x and Λ_y, are different.

x- or y-direction, the edge emission converges to ~3° only.

3. Structure design for enhanced edge emission

The symmetric NHA have been helpful for the mediation of extraordinary optical transmission through the nanoholes. However, it is not conducive to edge-emitting lasing action, since that would imply free-space radiation from all four edges of the structure, making the laser severely inefficient. Therefore, the structure shown in Fig. 1 needs redesigning for efficient edge emission, in addition to the surface emission. In this work, we take as recourse two approaches to enhance the edge emission. The first one is to change the periodicity of nanoholes to excite SPPs in one direction and suppress in the other. The second approach is to replace the periodic nanoholes by periodic grooves.

3.1. Restructuring NHA

This work aims to efficiently generate SPPs along the x-direction to enhance the edge emission in that direction. At the same time, the SPPs are expected to be suppressed along the y-direction to minimize loss.

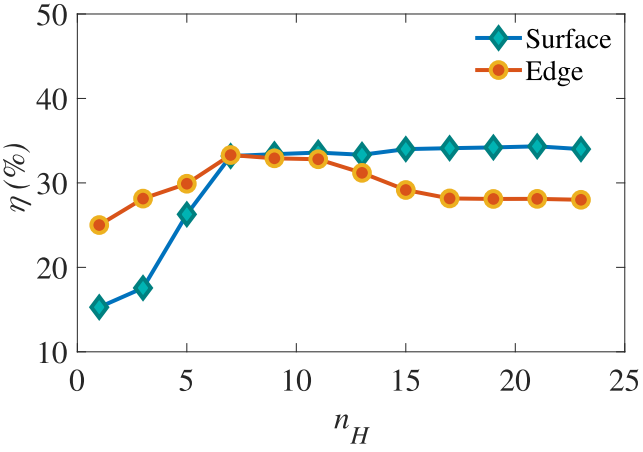

Fig. 6. Emission efficiency of vertical and edge-emitting modes plotted against the number holes (n_H) in the x-direction.

Such directional SPP excitation requires that the grating period (Λ_x) in the x-direction be equal to the SPP wavelength (λ_{SPP}), i.e., $\Lambda_x = \lambda_{SPP}$ [19]. This momentum-matching condition ensures that illuminations scattered across different holes interfere constructively with each other, thus increasing the efficiency of SPP excitation. The plasmonic peak sustained by the IR-140 dye molecules in this design is $\lambda_{SPP} = 870$ nm [6]. Therefore, we choose $\Lambda_x = 870$ nm and keep the NHA periodicity in the y-direction the same as before, i.e., $\Lambda_y = 350$ nm, as schematically shown in Fig. 5. The changes in the nanohole periodicity should limit the quadridirectional emission to bidirectional emission along the x-axis.

Next, we determine the number of nanoholes (n_H) along the x-direction that optimizes both surface and edge emissions. Too few holes would result in a weak surface emission, while too many of them would fail to contribute to the edge emission due to the short propagation length of SPPs [20]. Fig. 6 presents the lasing efficiency for both surface-

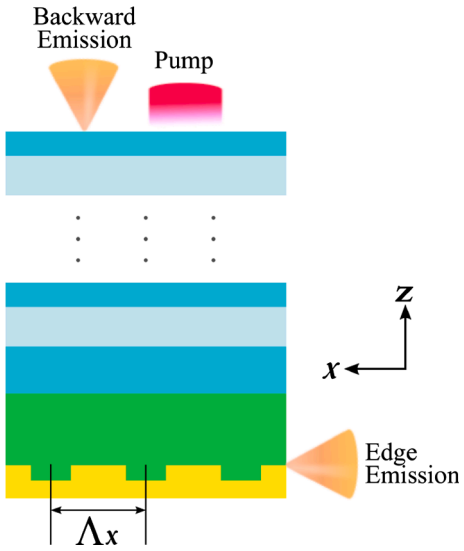

Fig. 7. 2D schematic illustration of the laser structure with periodically corrugated gold layer.

and edge-emitting modes against n_H in the x-direction. Since a significant portion of the pump energy scatters to the output on both occasions, a Gaussian filter centered at $\lambda_0 = 875$ nm is used to separate the lasing mode. Then the lasing mode is spectrally integrated to get the lasing power. Finally, the lasing efficiency is calculated by dividing the wavelength-normalized lasing power by the wavelength-normalized input pump power. We note that the surface-emission efficiency increases sharply for $n_H > 3$, since the spherical wavefronts emanating from each nanohole would interfere constructively to produce a spectrally coherent lasing mode [6]. The surface-emission efficiency does not change much for $n_H > 7$. By contrast, the edge-emission efficiency rises monotonically up to $n_H = 7$, remains relatively constant through $n_H = 11$, and then declines to a saturation level of ~28%. The dependence of edge-emission efficiency on n_H can be explained by the fact that near-IR SPP waves traveling along a gold-dielectric interface have a propagation length of ~2.5–5 μm [21]. Hence, the edge emission is not significantly impacted by SPPs propagating from distant holes. We also note that n_H works as a non-dynamic structural parameter to switch lasing from a surface-emitting operating mode to an edge-emitting operating mode, with $n_H = 7$ through 11 functioning as critical values to optimize both emissions. Hence, since the laser produces a slightly better overall result with $n_H = 11, n_H = 11$ has been chosen for the design and used in the calculations presented hereafter.

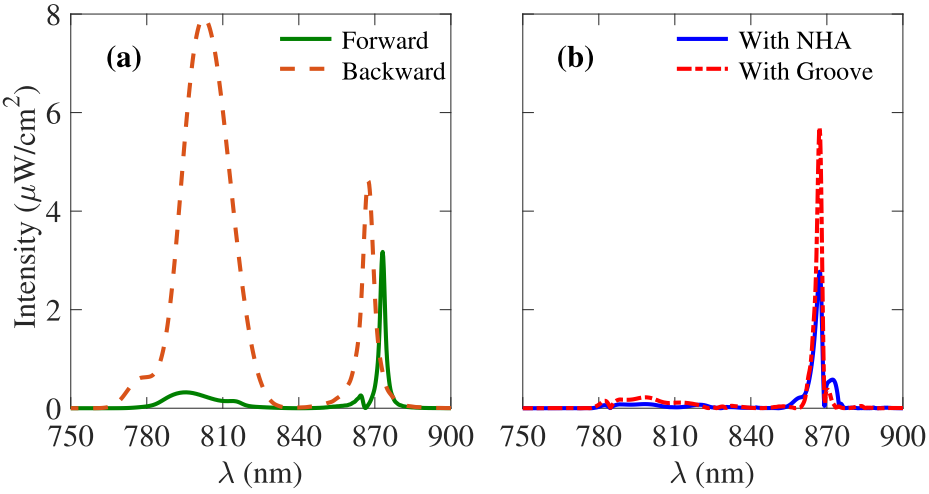

Fig. 8. (a) Forward surface emission with 2D NHA and backward surface emission with 2D grooves. (b) Edge emission with 2D NHA and with 2D grooves.

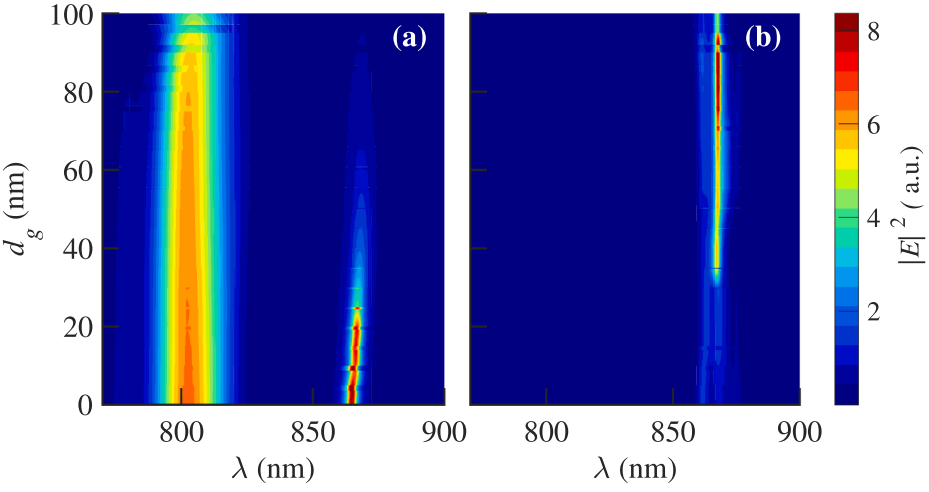

Fig. 9. $|E|^2$ distribution against groove depth (d_g) for (a) surface emission and (b) edge emission.

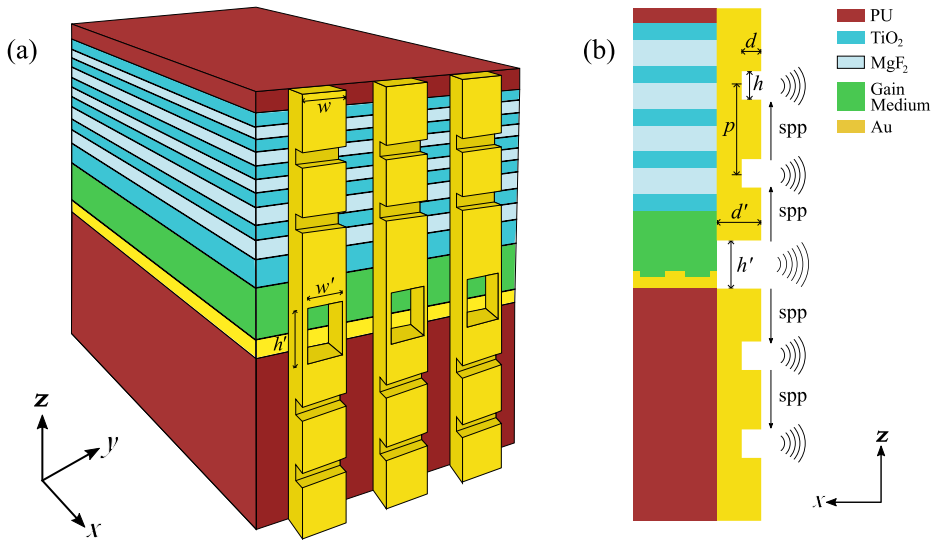

Fig. 10. Three-dimensional schematic illustration of the groove-aperture gold slab collimators mounted on the plasmonic laser's edge facet. (b) Cross-sectional view in the *x*-*z* plane showing different dimensional parameters of the collimators.

3.2. Replacing NHA by grooves

Now, the NHA is replaced by 2D periodic grooves filled with the gain medium, as schematically shown in Fig. 7. In the case of grooves, the metal layer is continuous throughout on the *x*-*y* plane. It does not let the incident light pass through it; instead, it reflects a significant part. Hence, using grooves instead of nanoholes shuts off the lasing in the forward direction but enhances backwards. The distributed Bragg reflector designed in this work also enhances the lasing in the backward direction. Additionally, grooves in the metal-dielectric interface reduce the wavevector mismatch between the radiative and surface-bound modes, resulting in the efficient generation and greater outcoupling of SPPs from the edge of the laser structure [22]. Fig. 8 shows lasing emission spectra from surface and edge with NHA and grooves. We note that grooves instead of NHA increase the lasing intensity both from surface and edge. The surface emission in the backward direction with grooves is stronger than that in the forward direction with NHA. The peak surface-emission wavelength in the backward direction with grooves is 867 nm, blue-shifted from that in the forward direction with NHA. We also note that the edge-emission intensity with grooves is significantly greater than that with NHA. Furthermore, the edge-emitting mode shows a relatively narrower linewidth than the surface-emitting mode. We also find that a significant fraction of the pump pulse accompanies the surface emission in the backward direction due to the Bragg mirror reflecting the pump pulse. The edge-emission output, on the other hand, almost does not include any pump energy.

The groove depth (d_g) presents another tunable parameter to optimize surface and edge emissions. We have investigated the frequency-resolved $|E|^2$ distribution against d_g, as shown in Fig. 9. As d_g increases, the surface emission starts strongly and then tapers off with a slight red-shifting behavior. This is because the surface emission in this plasmonic laser is mainly derived from SPP waves reflected from the array of grooves [23]. Planar SPP waves couple to gap plasmon modes inside the grooves and then re-radiate into free-space, having undergone a small red-shift with increasing groove depth. On the other hand, the edge emission is derived primarily from the direct outcoupling of SPPs. Therefore, no red-shifting is observed in the edge emission. We also find that the electric field intensity of reflected light is stronger at smaller wavelengths.

The edge-emitting mode centered at $\lambda_0 = 870$ nm manifests reverse characteristics. The edge emission is relatively weak for $d_g \lessapprox 30$ nm, and then it starts to get stronger. The edge-emission intensity is most vigorous when d_g is between 65 and 95 nm. We note that the location of the strongest surface-emission intensity does not coincide with that of the strongest edge-emission intensity. This non-overlapping characteristic of intense surface and edge emissions provides us with another structural parameter to switch between the two distinct modes of operation. However, $d_g = 35$ nm has been chosen in this work for simultaneous surface and edge emissions since this groove depth offers concurrent optimum radiation for both emissions.

4. Far-field collimation for edge emission

4.1. Collimator design

Conventionally, a meticulous arrangement of optical devices such as refractive lenses and mirrors can shape the far-field beam pattern [24]. However, such optical components are bulky and limit the fundamental purpose of compactness of plasmonic lasers. Hence, it is desirable to have a plasmonic laser with built-in beam collimation mechanisms. Here, a metallic groove-aperture plasmonic collimator has been proposed to be mounted onto the facet of the designed plasmonic laser to shape the far-field edge-emission beam pattern. Periodic textures surrounding a central slit on a metal slab can engineer the far-field pattern of edge-emitting light [25,26]. To date, such collimators have only been employed to shape the far-field laser beams of mid-IR and terahertz QCLs [27–29]. However, they have never been used in plasmonic lasers operating in the near-IR regime, making this work the first of its kind.

This work employs a groove-aperture structure carved on gold slabs integrated with the laser facet for collimating the far-field beam profile, as schematically shown in Fig. 10. An array of gold slabs—aligned with the grooves in the *y*-direction—cover the laser's entire lateral facet. An aperture exposes a portion of the gain medium and the metal-gain medium interface in each gold slab. The gold layers have symmetrical indentations on both sides of the central slit, as shown in Fig. 10(b). For the ease of integrating the gold slab collimators with the laser facet, additional PU layers are used beneath the gold layer and atop the PhC, which serve as a foundation onto which the gold slabs can be mounted. Without the dielectric padding layers above and below the core laser structure, the collimators would be suspended in air, making it a severe complication for the fabrication of the device.

In the longer wavelength limit, surface plasmons weakly couple to the metal-dielectric interface. These poorly confined plasmons are alternatively known as Zenneck waves, which are unsuitable to the task

Table 1
Optimal parameter values for the groove-aperture plasmonic collimator.

Parameter	Range Considered	Optimal Value
Groove periodicity (p)	750 nm $\leqslant p \leqslant$ 900 nm	845.80 nm
Groove height (h)	20 nm $\leqslant h \leqslant$ 100 nm	50.21 nm
Groove depth (d)	20 nm $\leqslant d \leqslant$ 100 nm	20 nm
Aperture height (h')	50 nm $\leqslant h' \leqslant$ 150 nm	50.21 nm
Aperture depth (d')	100 nm $\leqslant d' \leqslant$ 400 nm	225 nm
Aperture width (w')	100 nm $\leqslant w' \leqslant$ 350 nm	200 nm
Collimator width (w)	200 nm $\leqslant w \leqslant$ 350 nm	205 nm
Grooves on each side (n)	$1 \leqslant n \leqslant 5$	3

of plasmonic lensing. Hence, SPPs are recovered from Zenneck waves before plasmonic collimators can collimate the far-field beam pattern of mid-IR QCLs [30]. However, plasmonic lasers emitting near-IR light do not need such dispersion engineering because of the strong surface-bound nature of SPPs in the near-IR wavelength range [21].

The outgoing radiation via the aperture couples to surface plasmons that propagate along the metallic grating in the z-direction. The collimator groove periodicity (p) must be comparable to the emission wavelength (λ_0). As a result, the reradiated light waves from grooves reach the far-field in phase and interfere constructively to produce a highly focused central lobe [26]. The collimator groove height (h) and depth (d) need to be of deep subwavelength dimensions while the aperture height (h'), depth (d'), width (w'), and the collimator width (w) should be subwavelength for efficient wavefront engineering [26]. Additionally, the number of grooves (n) on each side of the aperture lends itself to tunability.

4.2. Optimized collimator

Since the output emission simultaneously depends on several parameters of the designed collimator, we have used the PSO technique to determine an optimal set of values for these structural dimensions. PSO is a robust, stochastic technique and has been extensively utilized in optical-geometric design-related problems [31,32]. The PSO algorithm converges on optimal solutions for a limited number of parameters by maximizing or minimizing a single figure-of-merit (FOM). Here, an optimized far-field emission requires a minimized full-width at half-maximum (FWHM) of the vertical divergence angle (θ_{vert}) and a maximized far-field peak intensity (E_{peak}) simultaneously. Therefore, an FOM can be defined to optimize the far-field edge-emission properties of the plasmonic laser, as given by

$$\text{FOM} = \frac{\theta_{\text{vert}}}{log_{10}|E_{\text{peak}}|}. \tag{1}$$

While minimizing the FOM of Eq. (1), the PSO algorithm minimizes θ_{vert} and maximizes E_{peak}. Since the collimator grooves are arranged in the vertical z-direction, the resulting collimation will be along the z-direction. The far-field pattern of the designed plasmonic laser's edge emission is already converged in the lateral direction. Therefore, 1D collimation in the z-direction is the objective in this work. Otherwise, a 2D plasmonic collimator can be used to achieve collimated far-field in both the vertical and lateral directions [29].

In this work, the PSO algorithm has been run over a broad range of the entire parameter set to determine the optimum parameter values that offer minimum FOM. The optimal parameters, along with the range considered for PSO, are given in Table 1. The collimators, designed with the optimal set of parameters, achieve a directional far-field pattern. Fig. 11(a) reveals that the far-field converges at an off-normal angle, which is typical for groove-aperture based collimation [33]. We also note from Fig. 11(b) that the lateral divergence pattern remains essentially identical. In contrast, Fig. 11(c) exhibits a significant change in convergence in the vertical direction with the use of collimators. FWHM of the principal lobe is ~4°, a nearly 45-fold reduction from the uncollimated beam. Furthermore, none of the secondary lobes exceeds 12% of the peak intensity, resulting in a small optical background [30].

4.3. Effects of groove parameters

The PSO Algorithm converges on an optimal solution set containing a

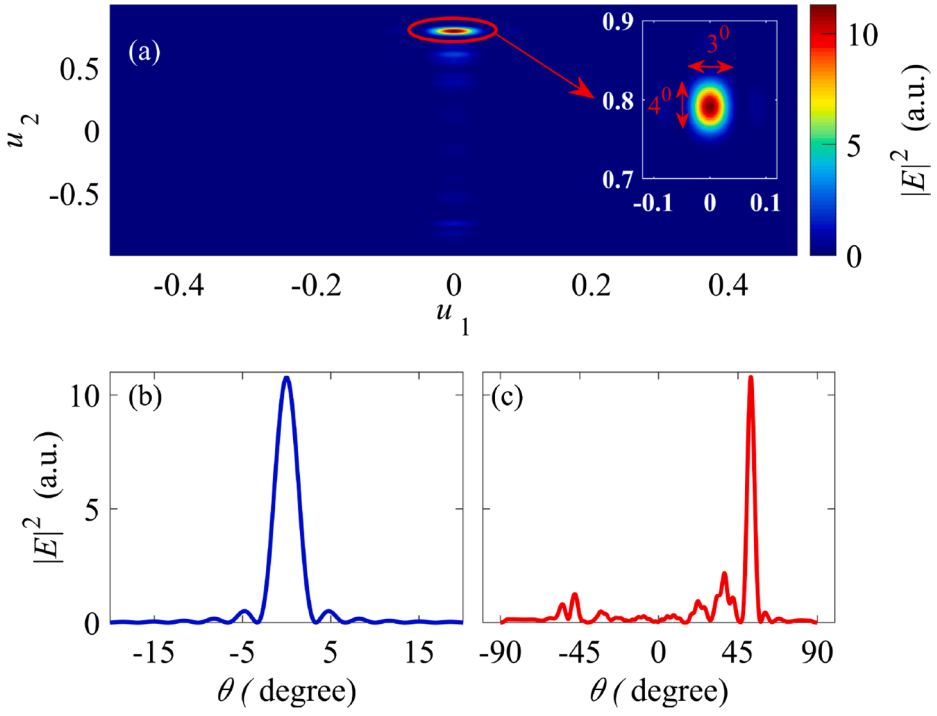

Fig. 11. (a) Far-field $|E|^2$ distribution at lasing wavelength with the optimized groove-aperture collimators. The inset reveals a 3°×4° beam spot. (b) Lateral divergence pattern in the y-direction and (c) vertical divergence pattern in the z-direction.

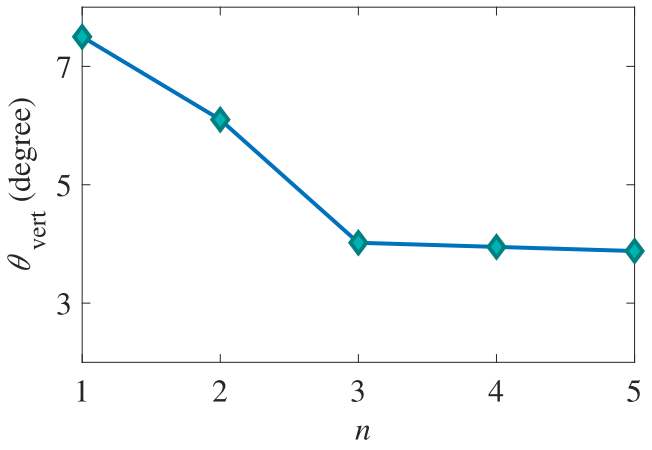

Fig. 12. The divergence angle (θ_{vert}) against the number of grooves on each side of the aperture (n).

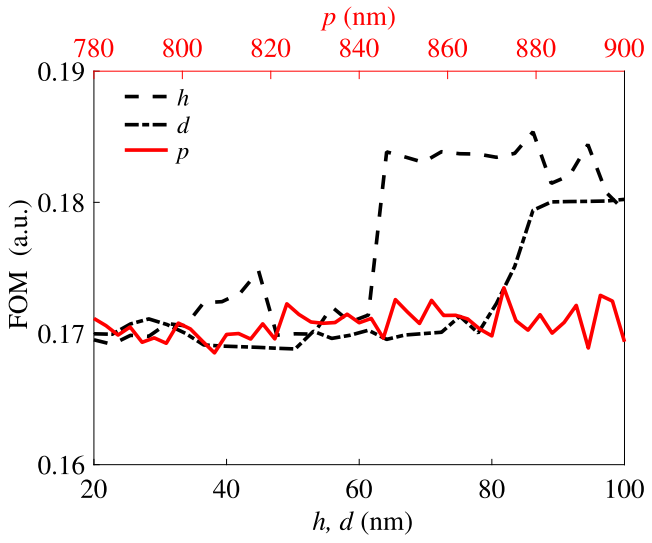

Fig. 13. FOM against the variations of groove height (h), depth (d), and periodicity (p).

local minimum for each parameter within a specified tolerance limit. In other words, the PSO algorithm is not infinitely efficient, and there is a satisfactory resolution within which it operates. Hence, there might be limited scope for improvement if a finer resolution is used. In this section, the effects of the individual groove parameters on the far-field collimation have been analyzed. It is worth noting that the groove parameters are significantly more critical in determining the far-field convergence than the aperture parameters [27].

In the groove-aperture plasmonic collimation approach, the convergence of the lasing emission depends on the number of grooves used on the collimator on each side of the aperture [29]. Conversely, the groove-aperture collimator, and hence, the laser structure becomes bigger as n increases. Hence, n is a crucially important parameter and requires an investigation to determine its effects on the collimation of the far-field beam pattern. Fig. 12 shows that θ_{vert} decreases drastically when $n = 3$ and does not change noticeably for $n > 3$. The fact that the far-field does not converge further with $n > 3$ can be attributed to the fast degeneration of near-IR SPP waves propagating along the gold-air interface beyond 2.5 μm [34]. Since $n > 3$ grooves fall beyond this critical length, they fail to significantly participate in the far-field beam shaping.

Fig. 13 shows the variation of the FOM as the groove parameters, such as height (h), depth (d), and periodicity (p), are varied. While one of the parameters is varied, other parameters are kept at their optimal values. FOM due to groove height remains relatively fixed up to $h = 60$ nm, and then it sharply increases. Similarly, the groove depth yields a smaller FOM up to $d = 80$ nm, beyond which FOM increases drastically. On the other hand, FOM shows only a slight dependence on groove periodicity. So long as p is reasonably close to the emission wavelength λ_0, satisfactory collimation is achieved. The values of the groove parameters at which the lowest FOM occurs match closely with those obtained by running the PSO algorithm, validating the optimized collimator designed using the PSO algorithm.

5. Conclusion

The near-IR planar plasmonic laser presented in this work manifests simultaneous surface- and edge-emitting lasing action. The edge emission from the designed planar plasmonic laser is found to be a lasing emission, although smaller than the surface emission when a 2D NHA is interfaced with the gain medium. A restructured plasmonic laser with the 2D NHA replaced by grooves enhances the edge emission. However, the edge emission is generally too diverge. A groove-aperture carved gold slab collimator has been designed and optimized to converge the far-field edge emission to only a $3^\circ \times 4^\circ$ spot. The simultaneous surface and edge emission from the designed plasmonic laser will open avenues for novel applications in nanoscale optoelectronic circuitry. The proposed plasmonic collimation for such nanoscale lasers will be essential for keeping the plasmonic lasers' dimensions within the nanoscale range and achieving a sharply converged edge-emission far-field beam pattern.

Declaration of Competing Interest

The authors declare that they have no known competing financial interests or personal relationships that could have appeared to influence the work reported in this paper.

References

[1] R.-M. Ma, R.F. Oulton, Applications of nanolasers, Nat. Nanotechnol. 14 (1) (2019) 12–22.
[2] C. Li, Z. Liu, J. Chen, Y. Gao, M. Li, Q. Zhang, Semiconductor nanowire plasmonic lasers, Nanophotonics 8 (12) (2019) 2091–2110.
[3] S.I. Azzam, A.V. Kildishev, R.-M. Ma, C.-Z. Ning, R. Oulton, V.M. Shalaev, M. I. Stockman, J.-L. Xu, X. Zhang, Ten years of spasers and plasmonic nanolasers, Light: Sci. Appl. 9 (1) (2020) 1–21.
[4] S.-L. Wang, S. Wang, X.-K. Man, R.-M. Ma, Loss and gain in a plasmonic nanolaser, Nanophotonics 1 (2020) no. ahead-of-print.
[5] C. Wu, S. Khanal, J.L. Reno, S. Kumar, Terahertz plasmonic laser radiating in an ultra-narrow beam, Optica 3 (7) (2016) 734–740.
[6] Z. Ahmed, M.A. Talukder, An efficient and directional optical tamm state assisted plasmonic nanolaser with broad tuning range, J. Phys. Commun. 2 (4) (2018) 045016.
[7] Z. Azad, M.S. Islam, M.A. Talukder, Mode-resolved analysis of a planar multi-layer plasmonic nanolaser, Opt. Commun. 482 (2020) 126614.
[8] M.A. Noginov, J.B. Khurgin, Miniature lasers: Is metal a friend or foe? Nat. Mater. 17 (2) (2018) 116–117.
[9] P.-P. Wang, S.-J. Yu, A.O. Govorov, M. Ouyang, Cooperative expression of atomic chirality in inorganic nanostructures, Nat. Commun. 8 (1) (2017) 1–9.
[10] T. Coenen, F.B. Arango, A.F. Koenderink, A. Polman, Directional emission from a single plasmonic scatterer, Nat. Commun. 5 (1) (2014) 1–8.
[11] R. Flynn, C. Kim, I. Vurgaftman, M. Kim, J. Meyer, A. Mäkinen, K. Bussmann, L. Cheng, F.-S. Choa, J. Long, A room-temperature semiconductor spaser operating near 1.5 μm, Opt. Express 19 (9) (2011) 8954–8961.
[12] Y. Jin, L. Gao, J.L. Reno, S. Kumar, High-power edge-emitting terahertz plasmonic quantum-cascade laser, in: 2019 Conference on Lasers and Electro-Optics (CLEO), IEEE, 2019, pp. 1–2.
[13] C. Holly, S. Hengesbach, M. Traub, D. Hoffmann, Simulation of spectral stabilization of high-power broad-area edge emitting semiconductor lasers, Opt. Express 21 (13) (2013) 15553–15567.
[14] A.J. Kuzma, Wafer-level test structure for edge-emitting semiconductor lasers, 2007. US Patent 7,180,929.
[15] M.V. Maximov, Y.M. Shernyakov, I.I. Novikov, L.Y. Karachinsky, N.Y. Gordeev, U. Ben-Ami, D. Bortman-Arbiv, A. Sharon, V.A. Shchukin, N.N. Ledentsov, et al., High-power low-beam divergence edge-emitting semiconductor lasers with 1-and 2-d photonic bandgap crystal waveguide, IEEE J. Sel. Top. Quantum Electron. 14 (4) (2008) 1113–1122.

[16] S.-H. Chang, A. Taflove, Finite-difference time-domain model of lasing action in a four-level two-electron atomic system, Opt. Express 12 (16) (2004) 3827–3833.
[17] Overcoming the multi-wavelength fdtd challenge, Sep 2018. https://www.lumerical.com/learn/whitepapers/overcoming-the-multi-wavelength-fdtd-challenge/ (accessed: 2021-01-15).
[18] M. Couture, Y. Liang, H.-P.P. Richard, R. Faid, W. Peng, J.-F. Masson, Tuning the 3d plasmon field of nanohole arrays, Nanoscale 5 (24) (2013) 12399–12408.
[19] I. Radko, S.I. Bozhevolnyi, G. Brucoli, L. Martín-Moreno, F. García-Vidal, A. Boltasseva, Efficient unidirectional ridge excitation of surface plasmons, Opt. Express 17 (9) (2009) 7228–7232.
[20] W.L. Barnes, Surface plasmon–polariton length scales: a route to sub-wavelength optics, J. Opt. Pure Appl. Opt. 8 (4) (2006) S87.
[21] A. Paul, D. Solis Jr, K. Bao, W.-S. Chang, S. Nauert, L. Vidgerman, E.R. Zubarev, P. Nordlander, S. Link, Identification of higher order long-propagation-length surface plasmon polariton modes in chemically prepared gold nanowires, ACS Nano 6 (9) (2012) 8105–8113.
[22] S.A. Maier, Plasmonics: fundamentals and applications, Springer Science & Business Media, 2007.
[23] M. Kuttge, F.J.G. de Abajo, A. Polman, How grooves reflect and confine surface plasmon polaritons, Opt. Express 17 (12) (2009) 10385–10392.
[24] F. Capasso, N. Yu, E. Cubukcu, E. Smythe, Using plasmonics to shape light beams, Opt. Photonics News 20 (5) (2009) 22–27.
[25] H.J. Lezec, A. Degiron, E. Devaux, R. Linke, L. Martin-Moreno, F. Garcia-Vidal, T. Ebbesen, Beaming light from a subwavelength aperture, Science 297 (5582) (2002) 820–822.
[26] L. Martin-Moreno, F. Garcia-Vidal, H. Lezec, A. Degiron, T. Ebbesen, Theory of highly directional emission from a single subwavelength aperture surrounded by surface corrugations, Phys. Rev. Lett. 90 (16) (2003) 167401.
[27] N. Yu, J. Fan, Q.J. Wang, C. Pflügl, L. Diehl, T. Edamura, M. Yamanishi, H. Kan, F. Capasso, Small-divergence semiconductor lasers by plasmonic collimation, Nat. Photonics 2 (9) (2008) 564–570.
[28] N. Yu, Q.J. Wang, M.A. Kats, J.A. Fan, S.P. Khanna, L. Li, A.G. Davies, E.H. Linfield, F. Capasso, Designer spoof surface plasmon structures collimate terahertz laser beams, Nat. Mater. 9 (9) (2010) 730–735.
[29] N. Yu, R. Blanchard, J. Fan, F. Capasso, T. Edamura, M. Yamanishi, H. Kan, Small divergence edge-emitting semiconductor lasers with two-dimensional plasmonic collimators, Appl. Phys. Lett. 93 (18) (2008) 181101.
[30] N. Yu, F. Capasso, Wavefront engineering of quantum cascade lasers using plasmonics, in: Plasmonics And Plasmonic Metamaterials: Analysis and Applications, World Scientific, 2012, pp. 123–166.
[31] M. Shokooh-Saremi, R. Magnusson, Particle swarm optimization and its application to the design of diffraction grating filters, Opt. Lett. 32 (8) (2007) 894–896.
[32] M. Awal, Z. Ahmed, M.A. Talukder, An efficient plasmonic photovoltaic structure using silicon strip-loaded geometry, J. Appl. Phys. 117 (6) (2015) 063109.
[33] S. Kim, H. Kim, Y. Lim, B. Lee, Off-axis directional beaming of optical field diffracted by a single subwavelength metal slit with asymmetric dielectric surface gratings, Appl. Phys. Lett. 90 (5) (2007) 051113.
[34] R. Dallapiccola, C. Dubois, A. Gopinath, F. Stellacci, L. Dal Negro, Near-field excitation and near-field detection of propagating surface plasmon polaritons on au waveguide structures, Appl. Phys. Lett. 94 (24) (2009) 243118.